Solar Trans-equatorial Activity

**Jingxiu Wang · Yuzong Zhang · Guiping Zhou ·
Louise K. Harra · David R. Williams · Yunchun Jiang**

Abstract We have found that solar flares in NOAA active region (AR) 10696 were often associated with large-scale trans-equatorial activities. These trans-equatorial activities appeared to be very common and manifest themselves through *i*) the formation and eruption of trans-equatorial loops (TELs), *ii*) the formation and eruption of trans-equatorial filaments (TEFs), and *iii*) the trans-equatorial brightening (TEB) in the chromosphere. It is determined that the TEF was formed following episodic plasma ejecta from flares occurring in the AR. The TEF eruption was associated with a trans-equatorial flare. All flares in the AR that were accompanied by trans-equatorial activities were associated with halo coronal mass ejections (CMEs). It was noticed that one or several major flares in the AR were followed by an increase of brightness and nonpotentiality of a TEL. These coupled events had a lifetime of more than 12 hours. In addition their associated halo CMEs always had a positive acceleration, indicating prolonged magnetic reconnections in the outer corona at high altitudes.

Keywords Sun: CME · Sun: trans-equatorial activity

1. Introduction

Solar prominences and flares were first detected in the 19th century. In 1971 coronal mass ejections (CMEs) were first detected by space observations (MacQueen *et al.*, 1974). How-

J. Wang (✉) · Y. Zhang · G. Zhou
National Astronomical Observatories, Chinese Academy of Science, Beijing 100012, China
e-mail: wangjx@ourstar.bao.ac.cn

Y. Zhang
Department of Astronomy, Beijing Normal University, Beijing 100875, China

L.K. Harra · D.R. Williams
University College London, Mullard Space Science Laboratory, Dorking, Surrey RH5 6NT, UK

Y. Jiang
Yunnan Astronomical Observatory/National Astronomical Observatories, Chinese Academy of
Sciences, Kuming 650011, China

ever, the importance of CMEs in the Sun – Earth connection has only been recognized since the 1990s (see Gosling, 1993).

Flares and many filament eruptions, which are often referred to as solar surface activities, occur on the scale of an active region (AR) whereas CMEs are large scale in nature. CME source regions cover a wider range of longitude and latitude than a single AR. Determining the source region of CMEs is an active topic of research (Munro *et al.*, 1979; Webb and Hundhausen, 1987; St. Cyr and Webb, 1991; Subramanian and Dere, 2001; Švestka, 2001; Zhang *et al.*, 2001, 2004; Hori and Culhane, 2002; Gopalswamy *et al.*, 2003; Zhou, Wang, and Zhang, 2003, 2006; Yashiro *et al.*, 2004; Vršnak, Sudar, and Ruždjak, 2005). These studies cover epochs from solar maximum to minimum using data sets from *Skylab*, SMM, and SOHO. They demonstrate the close association of CMEs with ARs and surface magnetic activity particularly in the form of the destabilization and eruption of prominences and their overlying coronal structures. Extended magnetic bipolar regions with complex ARs or long filaments inside, trans-equatorial loops, and trans-equatorial or polar crown filaments are found to be CME-prolific. There seems to be no distinction between flare-associated and non-flare-associated CMEs in acceleration or deceleration, which suggests that the cause may be different, possibly related to the nature of their source regions. The only differences are the magnetic field strength in the region of the field line opening and the velocity.

In recent studies large-scale magnetic sources of CMEs have been identified, with trans-equatorial loops (TELs) being one example (*e.g.*, Zhou, Wang, and Zhang, 2006). Trans-equatorial magnetic loops were first predicted by Babcock (1961) in his conceptual model of the solar magnetic cycle. However, the earliest detection of trans-equatorial loops was made with *Skylab* X-ray data (Chase *et al.*, 1976; Švestka *et al.*, 1977) in the early 1970s. The statistical properties of TELs were presented by Pevtsov (2000), Fárník, Karlicky, and Švestka (2001), and Chen, Bao, and Zhang (2006). Their flarelike behavior was reported by Harra, Matthews, and Driel-Gesztelyi (2003). Trans-equatorial loops have been identified to be large-scale source regions of some major Earth-directed halo CMEs (Khan and Hudson, 2000; Wang *et al.*, 2002; Glover *et al.*, 2003; Pohjolainen *et al.*, 2005a, 2005b). Statistically, approximately 40% of Earth-directed halo CMEs in solar cycle 23 are found to be associated with TELs (Zhou, Wang, and Zhang, 2006). In addition, trans-equatorial filaments (TEFs) and their surrounding magnetic fields were also suggested to be a source region of halo CMEs (Wang, 2002). Wang *et al.* (2006) demonstrated that the flare/CME event on the Bastille Day of 2000 was not a sole phenomenon of a single AR but was closely linked to a TEF and its sheared magnetic arcades. More than 13% of Earth-directed halo CMEs have been identified to be associated with TEFs (Zhou, Wang, and Zhang, 2006).

It has been noticed that in the large-scale magnetic composition of either TELs or TEFs, ARs often appear as an active component and seem to play an important role in the trans-equatorial activities. Active regions are often present in one or both lower legs of TELs or at one or both ends of the long filament channel of TEFs. Early in the *Skylab* era, the relationship between flares in ARs and the activity in TELs was studied by Švestka and Howard (1979, 1981) and Spicer and Švestka (1983). They suggested various interpretations of the brightening observed in TELs and implied some coupling of different scales in magnetic activity. Švestka and Howard (1979) argued that either flares or interconnecting loop brightenings were independent consequences of one common agent, presumably newly emerging flux. More recent investigations implied the interaction of multiscale magnetic flux systems in CME processes, in which TELs or inter-AR connections are an intrinsic ingredient (Wang *et al.*, 2002; Glover *et al.*, 2003; Maia *et al.*, 2003; Pohjolainen *et al.*, 2005a, 2005b; Liu, Webb, and Zhao, 2006; Wen *et al.*, 2006; Zhang *et al.*, 2007; Harra *et al.*, 2007). Coronal mass ejections seem to result from the magnetic coupling of scales from narrow reconnection current sheets to very large trans-equatorial connections.

The *Solar and Heliospheric Observatory* (SOHO) has provided solar observations of much improved resolution and sensitivity. The continuous temporal coverage and imaging capability of the Extreme ultraviolet Imaging Telescope (EIT; Delaboudiniére *et al.*, 1995), the Michelson Doppler Imager (MDI; Scherrer *et al.*, 1995), and the Large Angle and Spectrometric Coronagraph (LASCO; Brueckner *et al.*, 1995) are particularly useful for studying large- or global-scale events. In this paper we have studied the Sun – Earth connection events of November 2004 and found that flares in AR 10696 are often associated with trans-equatorial activities. During the observed period of 3 – 8 Nov., these trans-equatorial activities appeared frequently, manifested as formation and eruption of TELs, formation and eruption of TEFs, and trans-equatorial brightening in the chromosphere. In this interval, eight Earth-directed halo CMEs were detected by LASCO. They were all associated with coupled activity of flares and TELs (or TEFs). The complete sample of the active events in this interval offers us a good opportunity to carry out a detailed examination of solar trans-equatorial activity. In this study, two questions are addressed: *i*) what is the cause of trans-equatorial activities and the relationship between trans-equatorial activities and flares in AR10696? *ii*) What is the relationship between CMEs associated with flares and trans-equatorial activities? Could the interplay of the flares and trans-equatorial activities determine properties of the associated CMEs?

In the next section we introduce the data for our study. Sections 3 and 4 are devoted to the detailed description of the formation and eruption of TELs and TEFs, respectively. Section 5 is dedicated to the observed coupling of flares and trans-equatorial activities. In the final section we discuss our results.

2. Database and Data Analysis

We studied trans-equatorial activities in the period from 3 to 8 Nov. 2004. Our database predominantly comes from EIT, MDI, and LASCO onboard SOHO, as well as the Hα Telescope in Argentina (HASTA; Fernández Borda *et al.*, 2002), the Yunan Astronomical Observatory, the Big Bear Solar Observatory, and the Kanzelhöhe Solar Observatory.

The EIT observations that we analyzed are full-disk images using the 195 Å filter. All the EIT images were calibrated and derotated to the reference time at 23:46:58 UT on 6 Nov. The spatial resolution is estimated to be 5.2″.

EIT observations provide continuous temporal coverage of full-disk extreme ultraviolet (EUV) structures. Hence, most flares and eruptions can be identified from EIT images, even though the temporal resolution of the EIT observations is only 12 minutes.

Usually large-scale structures in the EIT images have a low intensity. To view the flaring in ARs and large-scale EUV structures simultaneously the EIT images have been renormalized to enhance the weaker emission. However, such renormalized EIT images are only used to show the morphology of the structure. For quantitative measurements, calibrated original images are used. The temperature distribution in the corona is estimated by using the line ratio of EUV 284 and 195 Å.

MDI five-minute-averaged full-disk magnetograms with a cadence of 96 minutes are used in this study. To understand three-dimensional (3-D) magnetic structures, constant-α force-free extrapolations are made based on the MDI magnetograms in the selected spatial window with the surface element method (Wang, Yan, and Sakurai, 2001). The force-free coefficient α is determined by fitting the extrapolated magnetic lines of force to the observed EUV structures.

Hα observations from the Yunnan Astronomical Observatory, the Big Bear Solar Observatory, the Kanzelhöhe Solar Observatory, and the Argentinean Observatory were co-aligned

with the space-borne data. From 4 to 8 Nov., with the exception of three C1 X-ray flares from AR 10691, the other 53 flares came from AR 10696. Therefore the GOES X-ray flux evolution in the studied interval can be predominantly considered as the light curve of flaring in AR 10696.

In the observation period, the Sun's magnetic fields were not too complicated. There were three ARs – AR 10693, 10695, and 10696. AR 10696 in the northern hemisphere increased in size and complexity, whereas the other two ARs (in the southern hemisphere) were decaying. The TEL became visible, connecting AR 10696 and AR 10695 on 3 Nov. It continued its activity in response to the magnetic evolution and flares of AR 10696 in the subsequent days. The TEL varied in brightness and nonpotentiality and erupted both partially and completely. In Figure 1, the typical appearance of the studied TEL and the TEF is show in EUV and Hα data, respectively. To show the relevant magnetic configuration more clearly, we present a smaller field of view MDI magnetogram for the selected window in Figure 2, on which contours of the TEL and TEF are superposed by red and yellow curves, respectively. In the northeast of the magnetogram, AR 10696 showed a compact quadrupole magnetic structure, and in the southwest of the figure, AR 10695 was embedded in a large area of positive flux of a coronal hole (see Harra *et al.*, 2007). The positive flux of AR 10696 and the coronal hole was in a slight conjunction, so that a large-scale magnetic neutral line went through the solar equator. The TEL connected the negative flux of AR 10696 and positive flux of AR 10695 and the coronal hole; the TEF was situated above the magnetic neutral line, which crossed the solar equator. In the period 6 – 7 Nov. both TELs and a TEF were present, allowing a comparison of the conditions for the formation and dynamics of these two types of trans-equatorial structures.

3. Formation and Eruption of Trans-equatorial Loops

A trans-equatorial loop is observed when loops connecting opposite hemispheres become visible (see Howard and Švestka, 1977). Magnetic connection can be persistent and survive for the whole disk passage of those connected ARs.

During the time interval 3 – 8 Nov., we can observe the life story of three TELs. A key characteristics of these TELs in this interval is that they all showed up above the EUV background in association with flare activity in AR 10696.

An example of the formation and eruption of the TEL on 4 Nov. is shown in Figure 3. Before 05:00 UT, there was no TEL signature connecting ARs 10696 and 10695 in the EIT images. The TEL appeared approximately at 05:46 UT following a B-class X-ray flare at 05:10 UT (see the X-ray light curve in the figure). After that the TEL was visible for approximately 18 hours. The TEL increased in intensity during and after the C1.0 flare at 07:23 UT. The TEL was sigmoidal from its early appearance. A flare with GOES class C6.3 took place in AR 10696 starting at 08:45 UT. The flare lasted more than one hour with a peak intensity at 09:05 UT. However, the remote flaring (see the brightening in the upper middle of the frame at 11:22 UT of the figure) to the northeast of the AR and the growing of postflare loops from the AR continued until 14:00 UT. This development could be identified clearly from EIT images from 11:22 to 13:24 UT in Figure 3. Co-temporally with the continuous growing of remote flare ribbons and postflare loops, the TEL increased in intensity, width, and nonpotentiality. Roughly from 19:00 UT, the TEL started to show an increase in intensity in its lower legs (see the EIT image at 20:09 UT). The C6.3 flare at 8:45 UT to the increase in intensity above the C flare threshold lasted about three hours, followed by a period of about 12 hours during which the X-ray flux showed a smoothly declining profile.

Figure 1 Upper panel: EIT image with a grid superposed at 17:11 UT on 6 Nov., showing a TEL, which is indicated by a red arrow. Lower panel: Hα image at 07:59 UT on 7 Nov. from Kanzelhöhe Solar Observatory, showing the TEF along the magnetic neutral line across the solar equator. Magnetic flux density contours of ±60 G from MDI at 17:35 UT on 6 Nov. are superposed on both images with yellow (red) contours for positive (negative) magnetic fields. These images shown are derotated to the same EIT image at 23:46:58 UT on 6 Nov., so that projection effects are partially corrected. A white box highlights the region of interest that will be studied in detail in Figure 2. For all figures north is at the top, and east at the left.
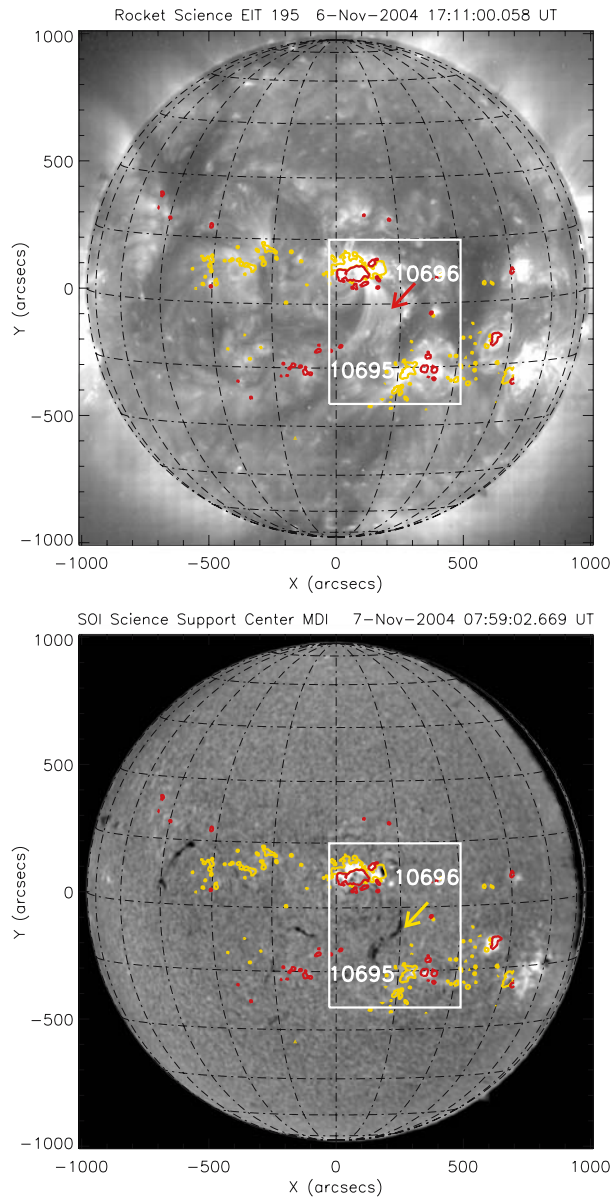
In Figure 4, we present the 3-D magnetic configuration by a constant force-free field extrapolation based on MDI magnetograms. The coefficient of force-free factor α is determined when extrapolated magnetic lines of force best match EUV structures in EIT images. The α for selected observations are 0.0001, −0.01, and −0.013 in units of arcsec^{-1}, respectively. Its absolute value shows an increase from 0.0001 to 0.013, indicating an increase in the magnetic nonpotentiality.

The continuous growing of brightness and flaring at the lower legs of the TEL took place in the course of the initiation and development of a halo CME (see the third CME
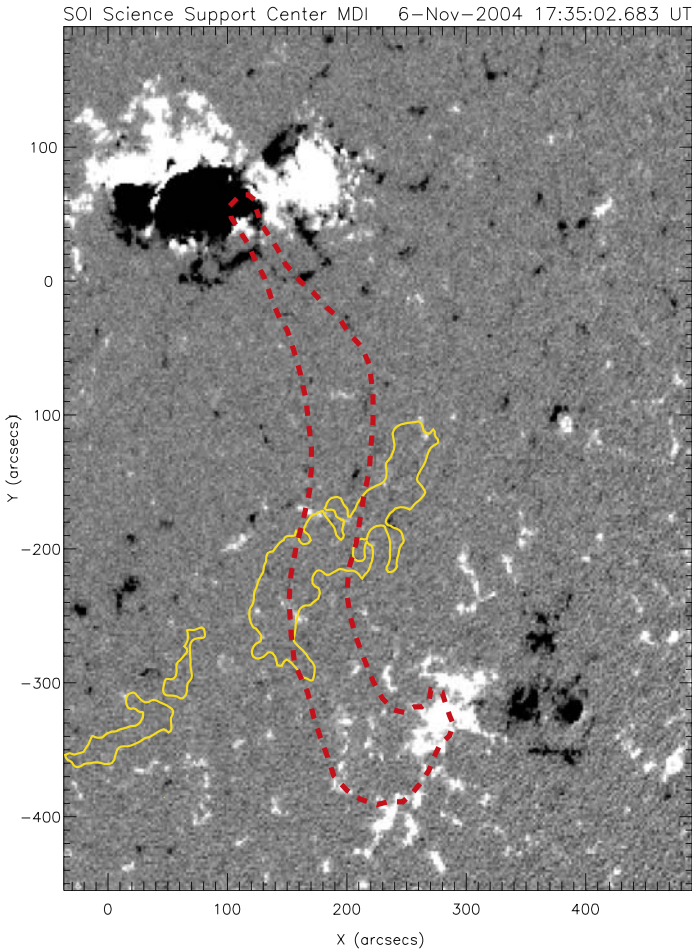
Figure 2 A smaller field of view of the MDI magnetogram (the boxed area shown in Figure 1). The outline of the TEL and TEF are shown by red dashed and yellow solid curves. The magnetogram is saturated at ± 100 G. AR 10696 is located in the northeast and AR 10695, in the southwest of the figure.

in Table 2). The brightening of the TEL resembled two-ribbon flares in the standard flare model with only one exception of a wide separation. This implies that energy input possibly came from persistent magnetic reconnection in the high corona. Thus, it is expected that the associated halo CME should have a long-lasting positive acceleration. The halo CME left the Sun at around 09:13 UT and was first observed in the LASCO C2 field of view (FOV) at 09:54 UT with an initial projective speed of 588 km s^{-1} (from the LASCO CME catalog). The interval from the CME initiation to its first appearance in C2 is shown as a shaded bar in the figure. The projected speed of the CME at 20 $R_\odot$ reached 706 km s^{-1}. The CME, indeed, showed an average positive acceleration of 6.3 m s^{-2}.

The TEL grew and remained during the whole CME process until the other two major flares in AR 10696 took place. The first M2.5 flare started at 21:42 UT and the second M5.4 flare at 22:53 UT. The second flare was accompanied by large-scale coronal dimmings. During the explosion of the second flare, the TEL erupted fully, and a halo CME appeared
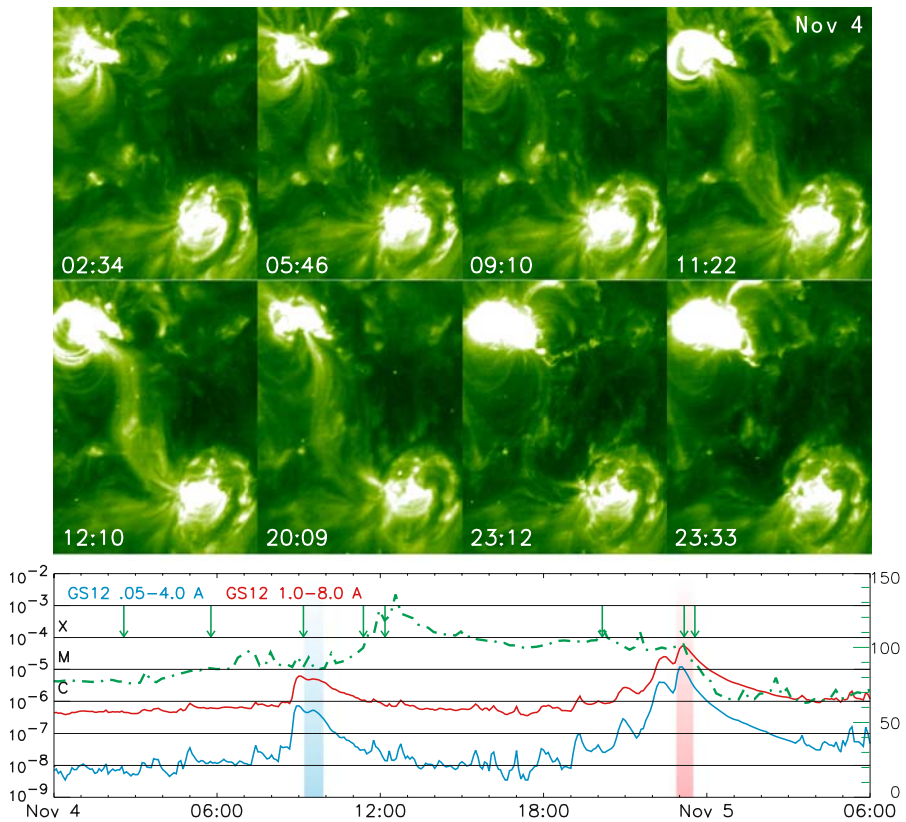
Figure 3 Upper panel: EIT images showing the formation and later eruption of a TEL. Lower panel: GOES soft X-ray flux changes in the energy bands of 0.05 – 4.0 Å (light blue) and 1.0 – 8.0 Å (red). The green arrows indicate the time of EIT images and shaded bars denote the interval of halo CME initiation on the solar disk and the first detection in LASCO C2 field of view. Dotted and dashed green curves in the lower panel indicate the averaged intensity for the TEL. Note the brightening in the lower legs of the TEL at about 20:09 UT.

at approximately the same time as the flare. This marked the end of the life story of the TEL. The flare-associated CME was first shown in the C2 FOV at 23:24 UT with an initial speed of 1055 km s^{-1}. The CME speed remained almost constant with a very small deceleration of -1.9 m s^{-2}. The lifetime of the two M-class flares was shorter than that of the C6.3 flare associated with the first halo CME.

It is noticed that the early eruption of the TEL was accompanied by an expanding brightening in the chromosphere. In Figure 5, an Hα filtergram from Big Bear Solar Observatory is shown in the right panel, in which bright points are marked by thin yellow contours. The trans-equatorial brightenings are similar to the sequential chromospheric brightenings reported by Balasubramanian *et al.* (2005), not only in their appearance but also in their dominant positive polarity (see the MDI magnetogram in the left panel of Figure 5). No corresponding trans-equatorial brightening could be seen in the closest EUV image at 23:09 UT; instead, the trans-equatorial darkening was observed from 23:21 UT in the EIT images. The trans-equatorial brightening is underneath the erupted TEL and the associated halo CME.

Figure 4 Left panel: Selected
EIT images. Right panel: 3-D
magnetic lines of force based on
a force-free field extrapolations
with constant α of 0.0001,
-0.01, and -0.013 arcsec^{-1},
respectively.
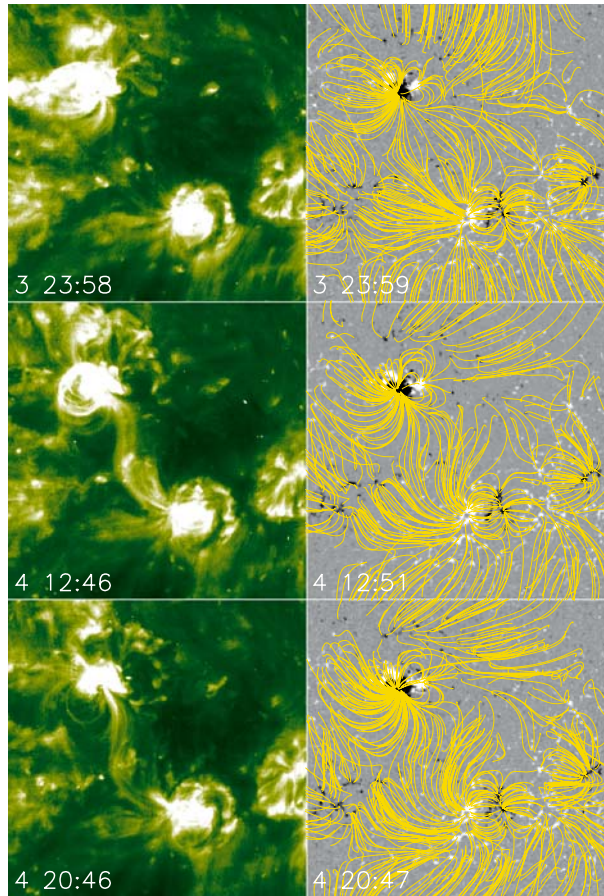
Figure 5 Right panel: An Hα
filtergram from Big Bear Solar
Observatory showing the
trans-equatorial brightening in
the chromosphere underneath the
erupted TEL. Left panel:
An MDI magnetogram at the
closest time to the
trans-equatorial brightening.
Bright points are marked by thin
yellow contours in the figure.
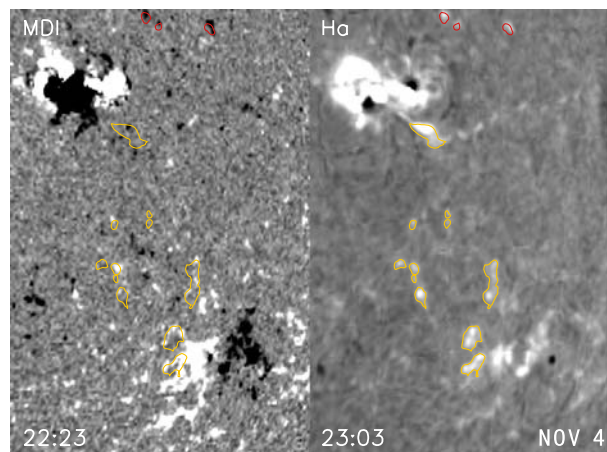
The observed scenario of the TEL activity can be summarized as follows:

 (i) The TEL appeared and grew following a few small flares at one of its lower legs in AR 10696.
 (ii) It brightened at the two lower legs after a long-duration C6.3 flare from 08:45 to 10:04 UT in the AR.
(iii) The long-duration flare and the growth of the TEL were associated with a halo CME of positive acceleration.
(iv) The TEL erupted during a major eruptive flare from 22:53 to 23:26 UT with significance of M5.4.
 (v) Trans-equatorial EUV dimming and brightening in the chromosphere took place during the early eruption of the TEL.
(vi) The eruptive flare and the eruption of the TEL correlated with a faster halo CME of small deceleration.

4. Formation and Eruption of a TEF

In the lower panel of Figure 1, a full-disk Hα filtergram shows a TEF along the large-scale magnetic neutral line extended from the neutral line of AR 10696 (also see Figure 2). The TEF is similar to the TEF associated with the Bastille Day flare/CME event of 2000 in which a large-scale magnetic neutral line extended from the neutral line of AR 9077 (Wang *et al.*, 2005, 2006). The filament reported by Balasubramanian *et al.* (2005) is also trans-equatorial.

We have examined all the available Hα observations from the Yunnan Astronomical Observatory, the Big Bear Solar Observatory, the Kanzelhöhe Solar Observatory, and HASTA and confirmed that the trans-equatorial filament in the studied interval appeared after 03:00 UT on 7 Nov. It was also identified without ambiguity that the TEF formed after a few episodes of bright plasma ejecta (Subramanian and Dere, 2001) from the western end of the magnetic neutral zone of AR 10696 in flares.

To illustrate details of the TEF formation, time sequences of Yunnan Hα images and running-difference images are shown in Figures 6 and 7, respectively. Yunnan full-disk Hα observations have a higher cadence of $1-3$ minutes, which enables us to study the formation of the TEF. These running-difference images show the ejection and propagation of hot ejecta and the later condensation in the formation of the TEF. In these running-difference Hα images from 02:45 to 03:03 UT, we saw bright ejecta after the C4.4 flare in AR 10696; later until 03:19 UT we observed darkening features tracing the propagating hot ejecta. The average propagation speed of the plasma ejection was 127 km s^{-1} as measured in Hα images in this period. The apparent darkening during this period can be interpreted as partially propagating and partially cooling of the ejected hot plasma. However, after 03:19 UT only darkening was observed in the magnetic neutral zone in Figures 6 and 7. We interpret this as cooling of the ejected hot plasma during the formation of the TEF. The processes leading to the formation of the TEF are briefly described in Table 1.

Subramanian and Dere (2001) have found that prominence eruptions are occasionally evident in EIT 195 Å data as cool prominence material seen in absorption or as bright ejecta seen in emission. In this study we identified many episodes of bright ejecta during flares in AR 10696 in 195 Å on-disk observations before the TEF formation. The first bright ejecta in the filament channel was found to be in the time window from 16:58 to 17:34 UT on 6 Nov. During the interval between 16:58 UT on 6 Nov. and the time of TEF eruption at 16:22 UT on 7 Nov. fourteen plasma ejections came from the AR into the filament channel. They were surgelike. In Figure 8, we only show four examples of plasma ejecta at 03:10,
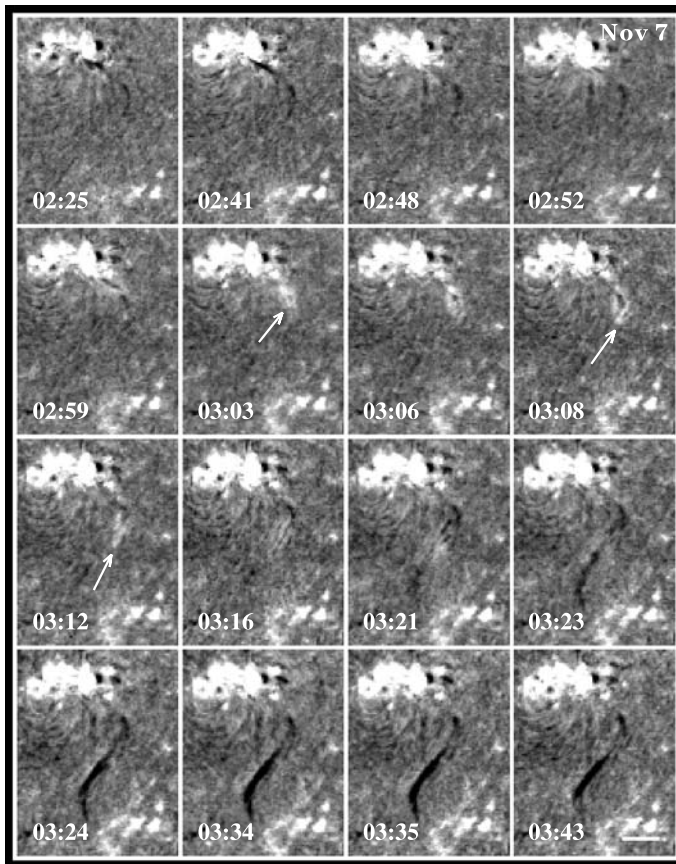
Figure 6 Time sequence of Yunnan Hα images showing the detailed process of the TEF formation. Arrows indicate the propagation of ejected plasma. The scale bar denotes a length of 100 arcsec.

05:34, 11:34, and 14:10 UT. The episodes of plasma ejection have an average duration of 37 ± 15 minutes in EIT observations. The available Hα observations covered intervals of seven ejecta. Figure 8 shows the formation and eruption of TEF by EUV running-difference images and Hα observations. Comparing Hα and EIT running-difference images, we found remarkable similarity in the appearances of EUV plasma ejecta and the Hα filament (see image pairs of 03:10 – 03:27, 05:34 – 06:51, 11:34 – 11:55, and 14:10 – 14:20 UT).

Figure 9 shows a comparison of simultaneous observations of the filament in Hα and EUV 195 Å wavelength. As Schmieder *et al.* (2004) showed, at EUV wavebands the dark filament channel was wider than that of the Hα filament. However, it is worthwhile mentioning that *the filament in the EIT image appeared in weak emission within the dark channel*. The EUV filament in weak emission has almost the same width as the Hα filament. It is likely that the dense plasma in the EUV filament channel only occupied a small volume. To confirm this, we deduced a coronal temperature map from the Fe XV and Fe XII line ratio, that is, EUV 284 to 195 Å data by using a line-ratio method (see Moses *et al.*, 1997, and reference therein). Results are shown in Figure 10 for periods before and well after the TEF formation. No 284 Å images are available at the time of filament formation. The TEF corresponded to lower temperature features in EUV. Moreover, the low-temperature features
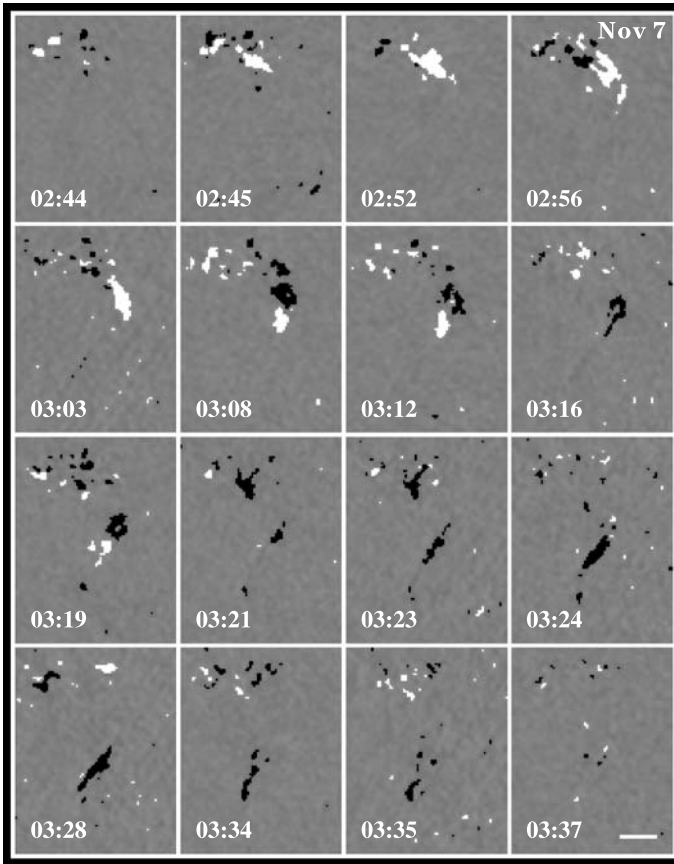
Figure 7 Time sequence of Hα running-difference images showing the propagation of ejected plasma in the processes of the TEF formation. The original Hα images have been smoothed with a flat background subtracted.

Table 1 Processes leading to the TEF formation on 7 Nov. 2004.

02:27 – 02:50	C4.4 flare
02:41	Surgelike ejection with two flaring knots at its base
02:59	Bright fringes appeared in the erupted filament
03:03	Ejected filament fully brightened
03:06	Darkening started in the ejected plasma
	while propagating southward
03:20	Continuous darkening of ejected plasma,
	and the TEF began to form
03:24	Early formation of the TEF

in EUV have a width similar to that of the Hα TEF and show sharp contrast to the higher temperature features of the channel.

The TEF formed after the plasma ejecta and continued changing its shape, width, and darkness in response to the ejecta from the AR in the next 12 hours. It finally erupted after
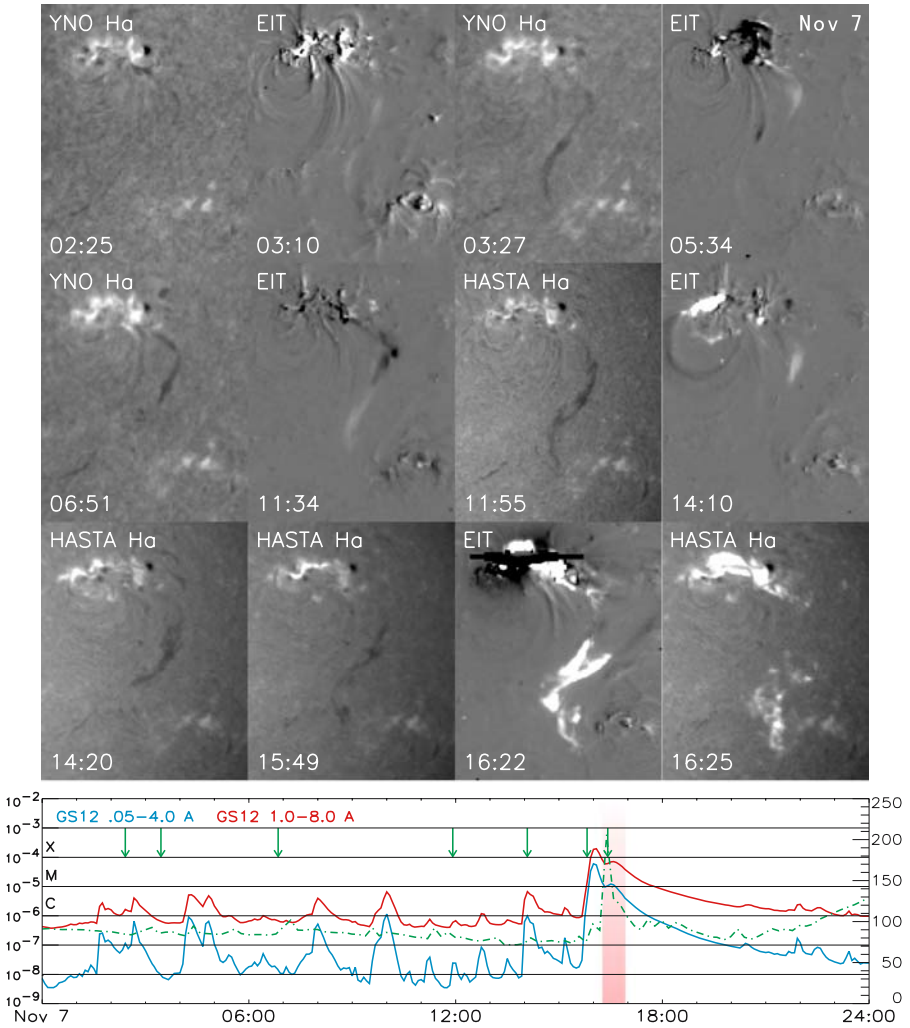
Figure 8 Time sequence composed by Hα images and EIT running-difference images showing the general aspects of the TEF formation and eruption. Green arrows superposed on the GOES X-ray light curve denote the time of the Hα images and shaded bars denote the interval of halo CME initiation on the solar disk and the first detection in LASCO C2 field of view. Dotted and dashed green curves in the lower panel indicate the averaged intensity of the EUV filament channel. Note the impulsive intensity increase of the filament channel during the trans-equatorial filament eruption.

the hot ejecta from 15:58 UT on 7 Nov. The TEF eruption resulted in a two-ribbon trans-equatorial flare in EUV (see image at 16:22 UT in Figure 8) and in Hα observations (see image at 16:25 UT in Figure 8). It is interesting to see that flaring patches in Hα were rather scattered, whereas the flaring at EUV was intense and compact, and appeared in the typical form of two ribbons. Eruption of the TEF and trans-equatorial flare were accompanied by a halo CME of clear deceleration (CME 7 in Table 2). On the solar disk large-scale trans-equatorial dimming was observed after the TEF eruption.

Figure 9 Fully developed TEF shown in Hα (left) and EIT images (right). Contours in the EIT image marks the position of the TEF seen in the Hα image.
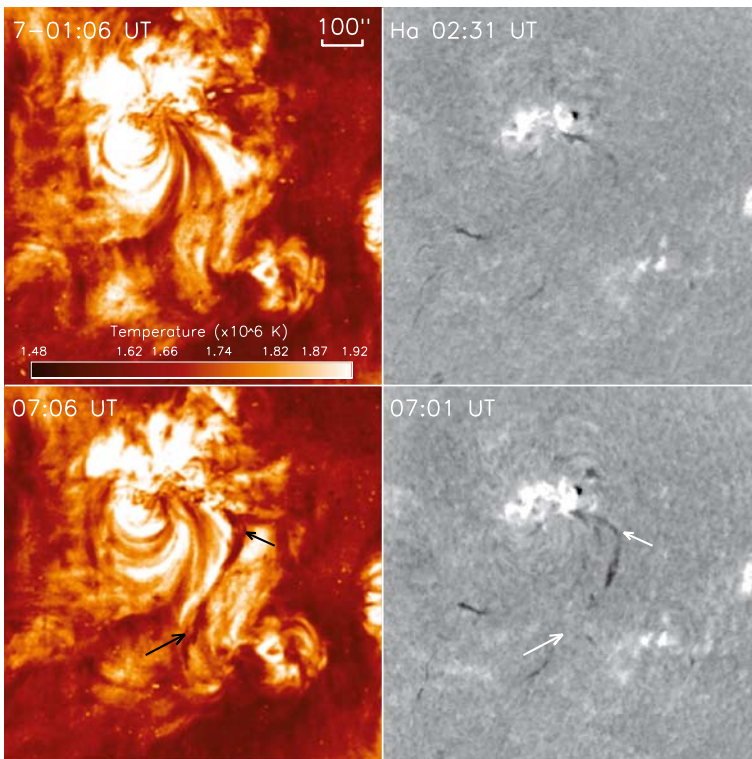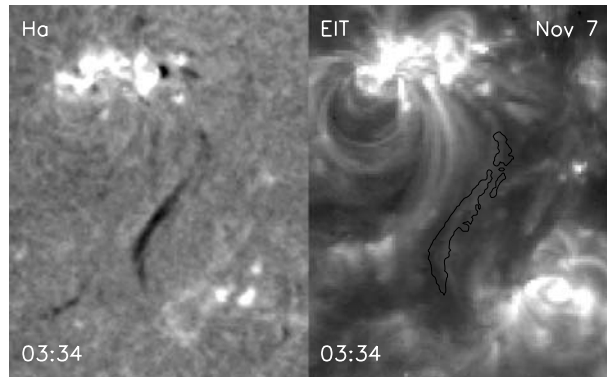
Figure 10 Hα images before and after TEF formation (right) and the corresponding temperature maps (left) deduced by the line ratio of 284 to 195 Å EIT data.

These observations raise an interesting issue: what is the mechanism of the TEF formation? In observations, the TEF formed by following the plasma ejecta from the flaring AR during the interval from 02:45 to 03:21 UT. The cooling time of the ejected plasma from the temperature of EUV and Hα emission to the Hα absorption is approximately 16 minutes (960 s) during the TEF formation (see Figures 6, 7, and 8). Considering the occurrence of many previous ejecta, we cannot exclude a longer cooling time. The cooling of hot flare

plasma has been studied by many authors (Culhane, Vesecky, and Phillips, 1970; Švestka, 1987; Cargill, Mariska, and Antiochos, 1995; Schmieder *et al.*, 1995; Warren *et al.*, 1999; Kamio, Kurokawa, and Ishii, 2003; López Fuentes, Klimchuk, and Mandrini, 2007). The data for this study do not allow a careful determination of the cooling process. According to Švestka (1987), within $3 \times 10^5 < T < 3 \times 10^7$ K, the conductive cooling is dominant from an analysis of order of magnitude, and the cooling time

$$t_{\mathrm{cooling}} = \int_{T(0)}^{T(t)} bT^{-\frac{7}{2}} \, \mathrm{d}T, \tag{1}$$

with $b = 2.66 \times 10^9 n_{\mathrm{e}}^{-1} L^2$, where L is adopted as the length of the TEF (*i.e.*, the scale of plasma cooling) and n_{e} is the plasma density taken as the value of the solar transition region and corona. The value of L can be determined based on Hα and EUV observations to be approximately 4×10^{10} cm. If we assume that $n_{\mathrm{e}} \approx 10^9$ cm^{-3} and T is 10^7 K, the cooling time would be approximately ≥ 800 s. From 3×10^5 to $T \simeq 2 \times 10^4$ K (Schmieder *et al.*, 1995), the radiative cooling would be too fast to take into account. The estimated cooling time is consistent in order of magnitude with the observed formation time of the TEF.

As a brief summary, an idea for TEF formation can be suggested as follows. The hot plasma was ejected from the flaring AR into the long magnetic neutral zone. The magnetic configuration of the filament channel can be a flux rope having 3-D magnetic dips as proposed by either Rust and Kumar (1994) or Aulanier *et al.* (1999). The ejected plasma was accumulated and supported either by concave parts of a flux rope or magnetic dips, accordingly. The accumulated hot plasma condensed by conductive and radiative cooling to produce the filament in the Hα waveband.

5. Global Coupling of AR Flares and Trans-equatorial Activities

The trans-equatorial solar activities have a close association with flares in the AR. We reveal the global coupling of flares in the AR and trans-equatorial events by focusing on more general aspects of solar activity. Examining the EUV images and the X-ray flux profile in Figure 3, we can get a general picture of the formation and development of a TEL, which started from a few flares in AR 10696. The whole episode seen in the X-ray profile seems to last more than 15 hours. An alternative view is that flares in the AR may only serve as parts of a general process of the TEL activity. This more global process certainly has a large-scale source magnetic region, and this global process manifests itself partially as a halo CME with positive acceleration in the outer corona.

In Figure 11, we show evidence of the global coupling by similar but more complicated TEL events than that of 4 Nov. (see Figure 3). They were related to two successive halo CMEs on 6 Nov. At 23:25 UT on 5 Nov., the TEL consisted of several sets of threads. Two M-class flares took place from 00:11 to 00:44 UT, respectively, accompanied by a partial eruption of the TEL and a halo CME with clear deceleration (CME 5 in Table 2). Then the third M-class flare appeared shortly from 01:40 UT, after which postflare loops grew and, at the same time, the TEL increased in width and brightness during the following 10 hours. Flaring of the TEL appeared at 08:11 UT in its southern lower leg (see the southern lower leg in the frame at 08:11 UT of Figure 11). At 14:23 UT on 7 Nov., the flare in the TEL lower legs reached its maximum phase. The whole process had a duration of more than 12 hours. The associated halo CME had a long-lasting acceleration. In the soft X-ray light curve, we saw an episode starting approximately from 00:00 to 14:30 UT on 6 Nov. with a smoothed profile containing no big eruptive changes.
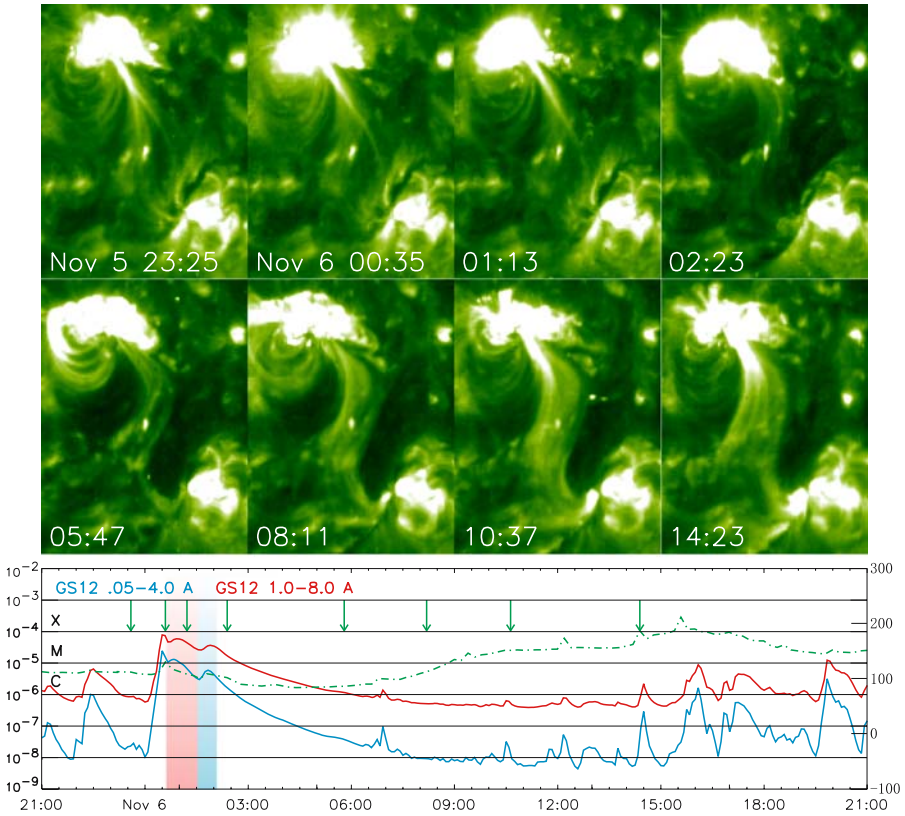
Figure 11 Time sequence of EIT images and X-ray light curves, showing the coupling of flares in AR 10696 and TEL activities. The drawing style of this figure is as the same as for Figure 3. Light curves of the TEL are shown by the green dotted and dashed lines.

To illustrate the increase of the brightness and the flaring in lower legs of the TEL, in Figure 12, we show dynamic changes of brightness in a time – position diagram. The ordinate of the right panel of Figure 12 denotes pixel position along the dashed line in the left panel from ARs 10696 to 695, and along the abscissa there are time slices of the brightness of the line from 00:00 to 15:00 UT. The partial eruption and the later brightening of the TEL can be seen clearly from approximately 02:00 UT, and the flaring in the two lower legs of the TEL started gradually from 06:00 UT and became very extensive at 09:00 and 12:00 UT in the southern and northern lower legs, respectively. The global brightening of the TEL is also shown by its light curves in Figure 11. The pronounced increase in the brightness started from 6:00 UT.

The gradual brightening of the TEL took place after 06:00 UT. The whole process of the flaring in the two lower legs of the TEL lasted many hours. The global coupling of the M3.6 flare in the AR and the continued development of the TEL together with the accelerated CME (CME 6 in Table 2) demonstrate the overall large-scale solar activity.

It is noticed that not all major flares in AR 10696 had their large-scale partners; but those that did have large-scale partners were CME-associated. In Table 2, we list all halo CMEs appearing in the interval 3 – 8 Nov. that were associated with flares in AR 10696 and trans-equatorial activities.
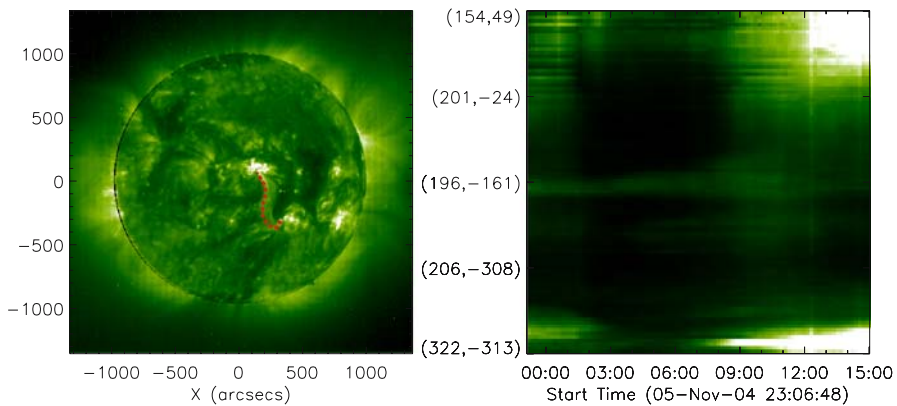
Figure 12 Time–position diagram showing brightness changes along the trans-equatorial loop as marked by the dashed red line in the left panel. In the right panel, the ordinate denotes pixel positions in (x, y) coordinates.

Table 2 CMEs and associated trans-equatorial activities. The first three columns are the order number, date, and CME initiation time, which are extrapolated by a linear fit to LASCO observations; the next column lists the corresponding flares in AR 10696; V and a express the CME initial speed (km s^{-1}) and acceleration (m s^{-2}).

CMEs			Flare	TA	V	a
1	3	03:12	M1.6 (03:23 – 03:57)	Unclear	918	−1.3
2	3	15:27	M5.0 (15:35 – 15:55)	Growing TL	1068	10.2
3	4	09:13	C6.3 (08:45 – 10:04)	Growing & flaring TL	653	6.3
4	4	22:50	M5.4 (22:53 – 23:26)	Eruption of TL & TB	1055	−1.9
5	6	00:38	M9.3 (00:11 – 00:42)	Partial eruption of TL	818	−81.5
			M5.9 (00:44 – 01:10)			
6	6	01:34	M3.6 (01:40 – 01:57)	Growing & flaring TL	1111	18.8
7	7	16:15	X2.0 (15:42 – 16:15)	Eruption of TF & TB	1759	−19.7
8	8	02:55	C7.9 (03:25 – 03:36)	Growing & flaring TL	462	7.8

Two points need to be emphasized:

 (i) The CMEs associated with a growing and/or flaring TEL always have positive acceleration (see CMEs 2, 3, 6, and 8 in Table 2), whereas those associated with the eruption of TELs or TEFs are decelerated (CMEs 4, 5, and 7). This result seems to shed new light on understanding why CMEs have different types of acceleration (see MacQueen and Fisher, 1983; Sheeley *et al.*, 1999). The growing and gradual flaring of TELs are likely to be evidence of the long-lasting magnetic reconnection in the outer corona, and the continued CME acceleration is a natural consequence of this long-lasting reconnection. The nature of this long-lasting reconnection requires further exploration.

(ii) The coupled activity of flares in the AR and trans-equatorial solar activities is associated with halo CMEs. Solar flares in the AR alone are not necessarily correlated with a global CME. In the studied interval there are twelve M-class flares and one X-class flare, among which six are not associated with halo CMEs. The latter were short-duration flares, with an average duration of 18 ± 9 minutes. The other eight $\geq$ M- and two C-class
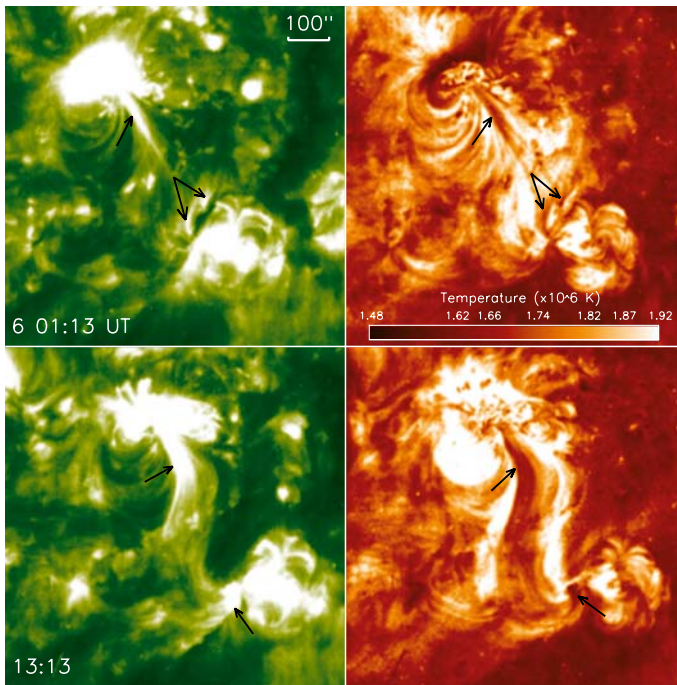
Figure 13 EIT 195 Å images (left) and their corresponding coronal temperature map (right) deduced from the line ratio of EIT 284 to 195 Å data.

flares that were associated with halo CMEs had an average duration of 37 ± 22 minutes, twice that of the former group. In addition, as illustrated by Table 2, flares associated with halo CMEs were accompanied by a type of trans-equatorial activity, but all non-halo-CME flares were clearly not accompanied by trans-equatorial activity.

6. Discussion and Conclusions

The key revelations of this study are briefly summarized as follows:

(i) Trans-equatorial solar activity is a common phenomenon that can be manifested as (1) formation, growth, and eruption of trans-equatorial loops, (2) formation, activation, and eruption of trans-equatorial filaments, and (3) trans-equatorial brightening in the chromosphere.

(ii) Flares in the flare-productive AR that were accompanied by trans-equatorial solar activities are also correlated with CMEs. All halo CMEs in the studied interval are associated with flares that were accompanied by trans-equatorial solar activity. However, no (even major) flare that was not accompanied by trans-equatorial solar activities is found to be correlated with halo CMEs.

(iii) A type of global coupling has been identified in which one or several major flares in the AR are followed by an increase in intensity and nonpotentiality of TELs and flaring of TELs in their lower legs. These coupled active events have a lifetime of more than 12 hours. Their associated CMEs always have positive acceleration, indicating

Figure 14 Cartoon showing a phenomenological idea of the TEL brightening.
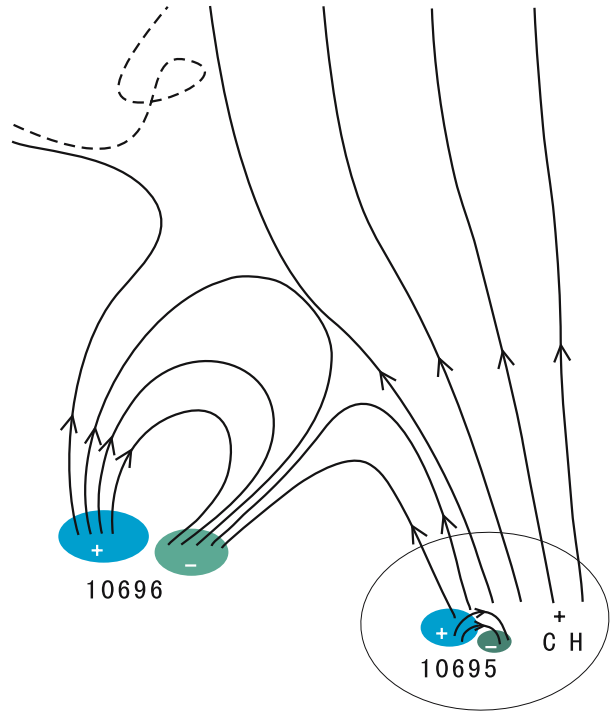
     long-lasting magnetic reconnections in the outer corona at gradually higher and higher altitudes.

(iv) The association of halo CMEs with the coupled activity of flares in the AR and the trans-equatorial solar activity indicates that halo CMEs have large-scale source regions. A single AR with its flare activity may not be capable of producing a CME with large angular width.

     The coupling of flares and trans-equatorial activities need to be further studied. Švestka and his co-workers explored this coupling in the late 1970s (see Švestka *et al.*, 1977; Švestka and Howard, 1979; and references herein). They suggested that the brightening of TELs could be influenced by flares in an associated AR in three ways: heat conduction, injection of accelerated particles, and evaporation of the flaring chromosphere. They also suggested that AR flares and the brightening of TELs might be connected by a common agent (*e.g.*, the flux emergence in the ARs). It is beyond the scope of this paper to discuss the physical mechanism or mechanisms of the TEL brightening. However, by using the method of the line ratio of EIT 284 and 195 Å data, we can roughly estimate the temperature distributions of the TEL (see Figure 13). Because the coronal plasma temperature map is obtained based on a set of assumptions, the determination of the temperature value is not very accurate. However, the temperature maps provide a very useful relative temperature comparison. The result shows that the TEL does not have a high temperature. The only interpretation of the brightening, then, is the increasing density in the TEL. The coincidence of bright surge-like brightening structures and low-temperature features in the lower legs of the TEL (see arrows in the figure) seems to be indicative of chromospheric evaporation. Following the scenario proposed by Harra *et al.* (2007), we suggest a phenomenological model of the TEL activity, which is illustrated by a cartoon of Figure 14. These expanding magnetic fields in

AR 10696 during the CME are continuously reconnecting with open fields of the coronal hole (partially including fields in AR 10695) to strengthen the TEL. The reconnection takes place at gradually higher and higher corona, which may contribute to the acceleration of the CME. Because the reconnection takes place in the very high corona, the heating within the TEL is not obvious, but it may cause the evaporation of chromospheric plasma into the TEL and hence the continuous brightening that was observed there.

It should be mentioned that another manifestation of large-scale activity is coronal waves shown by EIT observations, for which we have not made extensive analysis in this study. However, one fact is clear and interesting. For the coupled activity with growing and flaring in TELs, there were always coronal waves propagating on both sides of these TELs from the AR to large areas. These TELs became sigmoidal in shape as a syndromic response to the large-scale coronal disturbance. A good example is shown by EIT images of 02:23 UT and 05:47 UT in Figure 11. A further study is undertaken on the coronal waves in the studied interval.

References

Aulanier, G., Démoulin, P., Mein, N., van Driel-Gesztelyi, L., Mein, P., Schmieder, B.: 1999, *Astron. Astrophys.* **342**, 867.

Babcock, H.W.: 1961, *Astrophys. J.* **133**, 572.

Balasubramanian, K.S., Pevtsov, A.A., Neidig, D.F., Cliver, E.W., Thompson, B.J., Young, C.A., Martin, S.F., Kiplinger, A.: 2005, *Astrophys. J.* **630**, 1160.

Brueckner, G.E., Howard, R.A., Koomen, M.J., Korendyke, C.M., Michels, D.J., Moses, J.D., Socker, D.G., Dere, K.P., Lamy, P.L., Llebaria, A., Bout, M.V., Schwenn, R., Simnett, G.M., Bedford, D.K., Eyles, C.J.: 1995, *Solar Phys.* **162**, 357.

Cargill, P.J., Mariska, J.T., Antiochos, S.K.: 1995, *Astrophys. J.* **439**, 1034.

Chase, R.C., Krieger, A.S., Svestka, Z., Vaiana, G.S.: 1976, In: *Space Research XVI*, Akademie, Berlin, 917.

Chen, J., Bao, S., Zhang, H.Q.: 2006, *Solar Phys.* **235**, 281.

Culhane, J.L., Vesecky, J.F., Phillips, K.J.H.: 1970, *Solar Phys.* **15**, 394.

Delaboudiniére, J.-P., Artzner, G.E., Brunaud, J., Gabriel, A.H., Hochedez, J.F., Millier, F., Song, X.Y., Au, B., Dere, K.P., Howard, R.A., Kreplin, R., Michels, D.J., Moses, J.D., Defise, J.M., Jamar, C., Rochus, P., Chauvineau, J.P., Marioge, J.P., Catura, R.C., Lemen, J.R., Shing, L., Stern, R.A., Gurman, J.B., Neupert, W.M., Maucherat, A., Clette, F., Cugnon, P., van Dessel, E.L.: 1995, *Solar Phys.* **162**, 291.

Fárník, F., Karlicky, M., Švestka, Z.: 2001, *Solar Phys.* **202**, 81.

Fernández Borda, R.A., Mininni, P.D., Mandrini, C.H., Gómez, D.O., Bauer, O.H., Rovira, M.G.: 2002, *Solar Phys.* **206**, 347.

Glover, A., Harra, L.K., Matthews, S.A., Foley, C.A.: 2003, *Astron. Astrophys.* **313**, 285.

Gopalswamy, N., Shimojo, M., Lu, W., Yashiro, S., Shibasaki, K., Howard, R.A.: 2003, *Astrophys. J.* **586**, 562.

Gosling, J.T.: 1993, *Phys. Fluids* **B5**, 2638.

Harra, L.K., Matthews, S.A., van Driel-Gesztelyi, L.: 2003, *Astrophys. J.* **598**, 59.

Harra, L.K., Crooker, N.U., Mandrini, C.H., van Driel-Gesztelyi, L., Dasso, S., Wang, J., Elliott, H., Attrill, G., Jackson, B.V., Bisi, M.M.: 2007, *Solar Phys.*, in press.

Hori, K., Culhane, J.L.: 2002, *Astron. Astrophys.* **382**, 666.

Howard, R., Švestka, Z.: 1977, *Solar Phys.* **54**, 65.

Kamio, S., Kurokawa, H., Ishii, T.T.: 2003, *Solar Phys.* **215**, 127.

Khan, J.I., Hudson, H.S.: 2000, *J. Geophys. Res.* **27**, 1083.

Liu, Y., Webb, D.F., Zhao, X.P.: 2006, *Astrophys. J.* **646**, 1335.

López Fuentes, M.C., Klimchuk, J.A., Mandrini, C.H.: 2007, *Astrophys. J.* **657**, 1127.

MacQueen, R.M., Fisher, R.R.: 1983, *Solar Phys.* **89**, 89.

MacQueen, R.M., Eddy, J.A., Gosling, J.T., Hildner, E., Munro, R.H., Newkirk, G.A. Jr., Poland, A.I., Ross, C.L.: 1974, *Astrophys. J.* **187**, 85.

Maia, D., Aulanier, G., Wang, S.J., Pick, M., Malherbe, J.-M., Delaboudinière, J.-P.: 2003, *Astron. Astrophys.* **405**, 313.

Moses, D., Clette, F., Delaboudinière, J.-P., Artzner, G.E., Bougnet, M., Brunaud, J., Carabetian, C., Gabriel, A.H., Hochedez, J.F., Millier, F., Song, X.Y., Au, B., Dere, K.P., Howard, R.A., Kreplin, R., Michels, D.J., Defise, J.M., Jamar, C., Rochus, P., Chauvineau, J.P., Marioge, J.P., Catura, R.C., Lemen, J.R., Shing, L., Stern, R.A., Gurman, J.B., Neupert, W.M., Newmark, J., Thompson, B., Maucherat, A., Portier-Fozzani, F., Berghmans, D., Cugnon, P., van Dessel, E.L., Gabryl, J.R.: 1997, *Solar Phys.* **175**, 571.

Munro, R.H., Gosling, J.T., Hildner, E., MacQueen, R.M., Poland, A.I., Ross, C.L.: 1979, *Solar Phys.* **61**, 201.

Pevtsov, A.A.: 2000, *Astrophys. J.* **531**, 553.

Pohjolainen, S., Vilmer, N., Khan, J.I., Hillaris, A.E.: 2005a, *Astron. Astrophys.* **434**, 329.

Pohjolainen, S., Vilmer, N., Khan, J.I., Hillaris, A.E.: 2005b, In: *Proc. 11th European Solar Phys. Meeting – The Dynamic Sun: Challenges for Theory and Observations, 11 – 16 September 2005*, ESA SP-596, ESA, Noordwijk, 163.

Rust, D.M., Kumar, A.: 1994, *Solar Phys.* **155**, 69.

Scherrer, P.H., Bogart, R.S., Bush, R.I., Hoeksema, J.T., Kosovichev, A.G., Schou, J., Rosenberg, W., Springer, L., Tarbell, T.D., Title, A., Wolfson, C.J., Zayer, I.: 1995, *Solar Phys.* **162**, 129.

Schmieder, B., Heinzel, P., Wiik, J.E., Lemen, J., Anwar, B., Kotrč, E., Hiei, E.: 1995, *Solar Phys.* **156**, 337.

Schmieder, B., Lin, Y., Heinzel, P., Schwartz, P.: 2004, *Solar Phys.* **221**, 297.

Sheeley, N.R., Walters, J.H., Wang, Y.-M., Howard, R.A.: 1999, *J. Geophys. Res.* **104**, 24739.

Spicer, D.S., Švestka, Z.: 1983, *Solar Phys.* **87**, 271.

St. Cyr, O.C., Webb, D.F.: 1991, *Solar Phys.* **136**, 379.

Subramanian, P., Dere, K.P.: 2001, *Astrophys. J.* **561**, 372.

Švestka, Z.: 1987, *Solar Phys.* **108**, 411.

Švestka, Z.: 2001, *Space Sci. Rev.* **95**, 135.

Švestka, Z., Howard, R.: 1979, *Solar Phys.* **63**, 297.

Švestka, Z., Howard, R.: 1981, *Solar Phys.* **71**, 349.

Švestka, Z., Krieger, A.S., Chase, R.C., Howard, R.: 1977, *Solar Phys.* **52**, 69.

Vršnak, B., Sudar, D., Ruždjak, D.: 2005, *Astron. Astrophys.* **435**, 1149.

Wang, H., Yan, Y., Sakurai, T.: 2001, *Solar Phys.* **201**, 323.

Wang, J.X.: 2002, In: Hènoux, J.-C., Fang, C., Vilmer, N. (eds.) *Understanding Solar Active Phenomena*, International Scientific Publishers and World Publishing Corporation, Beijing, 157.

Wang, J., Zhang, J., Deng, Y.Y., Li, J.Q., Tian, L.R., Yang, X.L.: 2002, *Sci. China (Suppl.)* **45**, 57.

Wang, J., Zhou, G.P., Wen, Y.Y., Zhang, Y.Z., Zhang, J., Wang, H.N., Deng, Y.Y.: 2005, *Proc. IAU Symp.* **226**, 135.

Wang, J., Zhou, G.P., Wen, Y.Y., Zhang, Y.Z., Wang, H.N., Deng, Y.Y., Zhang, J., Harra, L.K.: 2006, *Chin. J. Astron. Astrophys.* **6**, 247.

Warren, H.P., Bookbinder, J.A., Forbes, T.G., Golub, L., Hudson, H.S., Reeves, K., Warshall, A.: 1999, *Astrophys. J.* **527**, L121.

Webb, D.F., Hundhausen, A.J.: 1987, *Solar Phys.* **108**, 383.

Wen, Y.Y., Wang, J.X., Mara, D.J.F., Zhang, Y.Z., Zhao, H., Zhou, G.P.: 2006, *Solar Phys.* **239**, 257.

Yashiro, S., Gopalswamy, N., Michalek, G., St. Cyr, O.C., Plunkett, S.P., Rich, N.B., Howard, R.A.: 2004, *J. Geophys. Res.* **109**, A07105.

Zhang, J., Kundu, M.R., White, S.M., Dere, K.P., Newmark, J.S.: 2001, *Astrophys. J.* **561**, 396.

Zhang, J., Dere, K.P., Howard, R.A., Vourlidas, A.: 2004, *Astrophys. J.* **640**, 420.

Zhang, Y.Z., Wang, J.X., Attrill, G.D.R., Harra, L.K., Yang, Z.L., He, X.T.: 2007, *Solar Phys.* **241**, 329.

Zhou, G.P., Wang, J.X., Zhang, J.: 2003, *Astron. Astrophys.* **397**, 1057.

Zhou, G.P., Wang, J.X., Zhang, J.: 2006, *Astron. Astrophys.* **445**, 1133.